

ՀՀ ԳԱԱ Ա.Բ. ՆԱԼԲԱՆԴՅԱՆԻ ԱՆՎԱՆ ԶԻՄԻԱԿԱՆ ՖԻԶԻԿԱՅԻ ԻՆՍՏԻՏՈՒՏ

ԱՐԹՈՒՐ ՄԱՆՎԵԼԻ ԱՂՅԱՆ

ՈՐՈՇ ԱՆՑՈՒՄԱՅԻՆ ՇԱՐՔԻ ՄԵՏԱՂՆԵՐԻ (IV-VI) ՆԱՆՈՉԱՓԱԿԱՆ ԿԱՐԲԻԴՆԵՐԻ ԵՎ
ԼԱՆԹԱՆԱՅԻՆ ՇԱՐՔԻ ՄԵՏԱՂՆԵՐԻ ԲՈՐԻԴՆԵՐԻ ՍԻԿՐՈԱԼԻԶԱՅԻՆ ՍԻՆԹԵԶ ԵՎ
ԿԱՏԱԼԻՏԻԿ ՀԱՏԿՈՒԹՅՈՒՆՆԵՐԻ ՈՒՍՈՒՄՆԱՍԻՐՈՒԹՅՈՒՆ

Բ.00.04- «Ֆիզիկական քիմիա» մասնագիտությամբ

քիմիական գիտությունների թեկնածուի գիտական աստիճանի հայցման ատենախոսության

ՍԵՂՄԱԳԻՐ

ԵՐԵՎԱՆ 2026

A.B. NALBANDYAN INSTITUTE OF CHEMICAL PHYSICS RA NAS

ARTUR M. AGHOYAN

MICROWAVE-ASSISTED SYNTHESIS AND INVESTIGATION OF THE CATALYTIC
PROPERTIES OF NANOSIZED CARBIDES OF TRANSITION METALS (GROUPS IV–VI) AND
BORIDES OF LANTHANIDE METALS

ABSTRACT

of Dissertation in 02.00.04 “Physical Chemistry” presented for the degree of
candidate of chemical sciences

YEREVAN 2026

Ատենախոսության թեման հաստատվել է ՀՀ ԳԱԱ Ա.Բ. Նալբանդյանի անվան Զիմիական ֆիզիկայի ինստիտուտի գիտական խորհրդում

Գիտական ղեկավար՝ քիմ. գիտ. դոկտոր Արգամ Վիլիկի Հակոբյան

Պաշտոնական ընդդիմախոսներ՝

քիմ. գիտ. դոկտոր, պրոֆ., Ռոմիկ Սուրենի Հարությունյան
տեխ. գիտ. թեկնածու Վոլոդյա Վազգենի Բաղդամյան

Առաջատար կազմակերպություն

Երևանի Պետական Համալսարան

Պաշտպանությունը կայանալու է **2026թ. փետրվարի 23-ին ժ. 14:30-ին, ՀՀ ԳԱԱ Ա. Բ. Նալբանդյանի անվան Զիմիական ֆիզիկայի ինստիտուտում** գործող ՀՀ ԲԿԳԿ-ի 017

<< քիմիա >> մասնագիտական խորհրդում (0014, Երևան, Պ. Սևակի փողոց, 5/2):

Ատենախոսությանը կարելի է ծանոթանալ ՀՀ ԳԱԱ Ա.Բ. Նալբանդյանի անվան Զիմիական ֆիզիկայի ինստիտուտի գրադարանում:

Սեղմագիրն առաքված է 2026թ. հունվարի 22-ին:

017 Մասնագիտական խորհրդի
գիտական քարտուղար, ք.գ.թ



Մարիետա.Կ. Չաքարյան

The subject of the dissertation is approved by the scientific council of the A.B. Nalbandyan institute of Chemical physics, NAS RA

Scientific advisor:

Doctor of chemical sciences Argam V. Akopyan

Official opponents:

Doctor of chemical sciences, professor Roomik S. Harutunyan

Candidate of technical sciences Volodya V. Baghramyan

Leading organization:

Yerevan State University, Armenia Yerevan

Defense will take place on **23st of February 2026 at 14:30 o'clock**, on meeting of the "Chemistry" professional council's session of the HESC RA 017 acting within the Institute of Chemical Physics after A.B. Nalbandyan NAS RA (0014, Yerevan, P. Sevak str., 5/2).

The PhD thesis is available at the library of A.B. Nalbandyan Institute of Chemical Physics the NAS RA.

The abstract is sent out on January 22, 2026.

Scientific secretary of the 017 special council,
Candidate of Chemical Sciences



Marieta K. Zakaryan

GENERAL DESCRIPTION OF THE WORK

General introduction

The development of efficient, sustainable, and economically viable catalysts and refractory materials is a key challenge in modern materials science and heterogeneous catalysis, driven by the need for cleaner fuels, stricter environmental regulations, and the transition toward renewable carbon resources. Advanced catalytic systems must operate under mild conditions while maintaining high activity, selectivity, and long-term stability.

Transition-metal carbides and boron-rich compounds exhibit a unique combination of metallic, covalent, and ionic properties, providing high thermal stability, electrical conductivity, and noble-metal-like catalytic behavior. These materials have emerged as promising, cost-effective alternatives to precious metals in hydrogenation, hydroprocessing, oxidation, and biomass conversion reactions.

However, conventional synthesis methods for carbides and borides are typically energy-intensive, time-consuming, and require extreme temperatures or hazardous atmospheres, often offering limited control over phase purity, particle size, and surface chemistry. Microwave-assisted synthesis overcomes many of these limitations by enabling rapid volumetric heating, accelerated reaction kinetics, reduced energy consumption, and access to nanostructured and metastable phases.

This dissertation focuses on the development of microwave-assisted routes for synthesizing lanthanide hexaborides, boron monophosphide, transition-metal carbides, including mixed/synergistic carbide catalysts, and on establishing clear structure–property–performance relationships. Particular emphasis is placed on catalytic applications relevant to clean fuel production, especially in oxidative desulfurization and biomass upgrading related processes (hydrogenation, hydrodeoxygenation).

Aim and objectives of the work

The main aim of this dissertation is to develop rapid, energy-efficient microwave-assisted synthesis routes for refractory borides and transition-metal carbides and to investigate their structure–property–activity relationships in heterogeneous catalytic processes.

To achieve this aim, the following objectives were addressed:

- Develop simple, rapid, and energy-efficient microwave-assisted synthesis routes for series lanthanide hexaborides and boron monophosphide, and to evaluate their phase formation, structural, and physicochemical characteristics.
- Optimize synthesis parameters using domestic microwave oven to obtain nanosized powders with narrow particle size distributions and tailored surface properties, while significantly reducing synthesis temperature and duration compared to conventional furnace-based methods.
- Synthesize nanosized transition-metal carbides using microwave irradiation and systematically investigate the influence of synthesis parameters on phase composition, particle size, morphology, and surface chemistry.
- Design mixed and synergistic carbide catalysts based on multimetallic systems and elucidate the role of metal–metal and metal–carbon interactions in governing catalytic activity and selectivity.

- Establish correlations between surface properties (oxidation states, acidity, electronic structure, and metal dispersion) and catalytic performance using comprehensive physicochemical characterization.
- Evaluate the catalytic activity, selectivity, and stability of the synthesized carbide materials in key model reactions, including hydrogenation and aerobic oxidation.

The scientific novelty of the work

- For the first time, microwave-assisted solid-state synthesis was systematically applied to the preparation of lanthanide-series metal hexaborides and boron monophosphide.
- Microwave irradiation was employed for the synthesis of transition-metal carbides, including single-phase carbides as well as doped and mixed (multimetallic) carbide systems.
- For the first time, a comprehensive and systematic correlation between synthesis conditions and catalytic properties of the obtained carbides was established, revealing the influence of microwave synthesis on particle size, surface active sites, and microstructural features.
- For the first time, the high catalytic efficiency of mixed and synergistic transition-metal carbides was demonstrated in aerobic oxidative desulfurization, both in model reactions and in straight-run gasoline fractions.
- The synthesis and catalytic evaluation of molybdenum carbide with tunable activity and selectivity, controlled by microwave synthesis parameters, were investigated in model naphthalene hydrogenation reaction.
- A dual-functionality concept for carbide-based catalysts-combining acidic sites and hydrogen-activating centers was experimentally validated.

The practical importance of the paper

The microwave-assisted solid-state synthesis strategy developed in this work demonstrates high scalability potential and provides an energy-efficient route for the preparation of structurally homogeneous nanomaterials with narrow particle size distributions and controlled surface properties. The proposed approach enables the synthesis of highly active, selective, and stable transition-metal carbide-based catalysts, whose performance was successfully validated under continuous-flow conditions closely approximating industrial operation. Moreover, microwave irradiation makes it possible to access thermodynamically “challenging” and kinetically hindered inorganic systems, including lanthanide-series hexaborides and boron monophosphide, thereby highlighting the versatility, robustness, and broad applicability of microwave-assisted solid-state synthesis for advanced functional materials.

Content and structure of the work

The dissertation consists of an introduction, four chapters, conclusions and a list of references. It is composed within 150 pages, includes 8 charts, 56 pictures and 316 references.

Publications

The main part of the dissertation has been published in six (6) articles in high-impact international peer-reviewed journals, one of which was published without co-authors. The results of the studies have been reported in international and local scientific conferences.

Acknowledgement

This dissertation was largely supported by the State Committee of Science of the Republic of Armenia within the framework of Grant [# 22RL-007].

THE MAIN CONTENT OF THE DISSERTATION

The primary description, clauses, reasoning and aim of the paper, its relevance, scientific novelty, practical importance, obtained results, their discussion and corresponding conclusions are presented in the dissertation.

Chapter 1. Literature review: Chapter 1 presents a comprehensive and up-to-date literature review focused on microwave-assisted solid-state synthesis and functional refractory materials such as hexaborides and transition metal carbides. The chapter critically discusses the fundamental mechanisms of microwave–solid interactions (primarily at 2.45 GHz), emphasizing the intrinsic differences between microwave and conventional thermal heating, including volumetric energy absorption, selective heating, accelerated kinetics, and non-equilibrium effects. The advantages and limitations of microwave processing are evaluated in comparison with traditional solid-state, carbothermal, borothermal, and gas-phase methods. Particular attention is given to transition-metal carbides (TMCs) as a strategically important class of catalytic materials with noble-metal-like behavior, as well as to lanthanide hexaborides, boron monophosphide highlighting their physicochemical properties, and the synthetic challenges associated with conventional high-temperature routes. The review demonstrates that microwave irradiation offers unique opportunities for overcoming kinetic and thermodynamic barriers, especially for the synthesis of nanostructured carbides and borides, whose controlled preparation remains difficult using classical heating techniques.

Chapter 2. Experimental section: This chapter details the experimental procedures applied throughout this dissertation. Microwave-assisted synthesis method (MS) was carried out using stoichiometric mixtures of metal oxides (transition-metal or lanthanide oxides) with appropriate solid reactants such as carbon, boron, or phosphorus-containing (for synthesis of boron monophosphide BP) precursors. The homogenized raw mixtures were placed into a silica (quartz) flow-type microwave reactor (Figure 1) and irradiated under inert (N_2 or He) atmospheres. The reaction temperature in the incandescence zone was monitored in situ using an optical pyrometer (Dostman HT 1800), ensuring reliable control of the synthesis process.

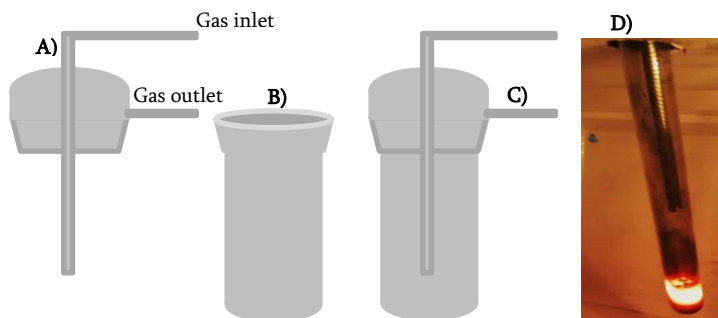


Figure 1: Quartz flow reactor A) Quartz lid equipped with gas purging system, B) quartz reactor, C) Quartz reactor equipped with gas purging system, D) photo of quartz-flow reactor containing raw mixture during microwave heating.

The obtained materials were comprehensively characterized using a combination of structural, morphological, surface, and textural techniques, including XRD, SEM/EDS, TEM, XPS, N_2 -

adsorption/desorption and BET surface area measurements, temperature-programmed reduction and desorption analysis (H₂-TPR, NH₃-TPD) methods. Transition-metal carbides were subsequently evaluated in model and real catalytic reactions, such as hydrogenation and oxidative desulfurization, using batch and flow reactor setups. Reaction products were analyzed mainly by gas chromatography (GC-FID and GC-MS) with absolute calibration methods. Particular emphasis was placed on establishing correlations between synthesis conditions, physicochemical properties, and catalytic activity, selectivity, and stability, providing a rational basis for catalyst design.

Chapter 3. Microwave-assisted synthesis and characterization of lanthanide hexaborides and boron monophosphide: In this chapter, the feasibility of synthesizing boron monophosphide and lanthanide (rare-earth) hexaborides under microwave irradiation is demonstrated and systematically discussed.

Boron monophosphide (BP): Despite of the outstanding properties of boron monophosphide (BP), its broad utilization is limited by the complexity of its synthesis. Boron monophosphide (BP) nanopowder for the first time was synthesized by a microwave-assisted solid-state route using

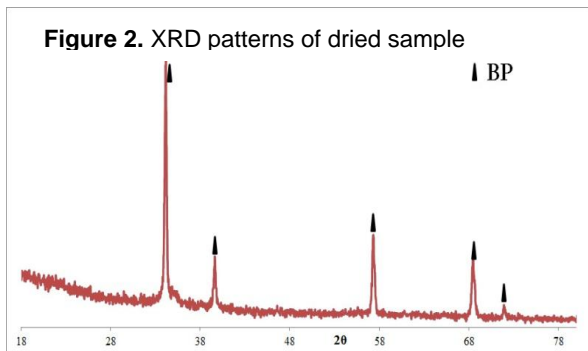
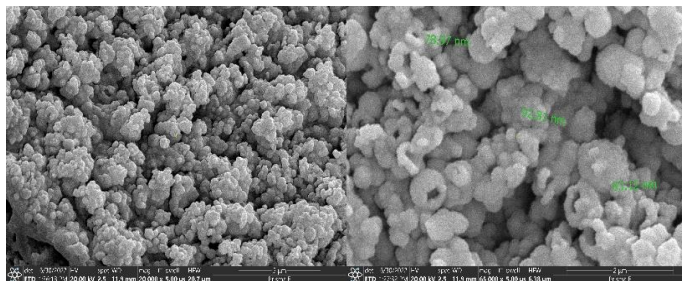


Figure 3. SEM images of dried samples



readily available oxide and elemental boron precursors. Several precursor systems, including (NH₄)₃PO₄ + B, BPO₄ + B, and P₂O₅ + B, were initially evaluated, among which the stoichiometric P₂O₅ + B mixture was identified as optimal. After thorough homogenization, the powder mixture was transferred into a quartz gas-flow reactor and subjected to microwave irradiation for 10 min under a continuous nitrogen flow of 20 mL·min⁻¹. During irradiation, the temperature in the incandescent reaction zone was monitored using an optical pyrometer and did not exceed 900 °C. The synthesis proceeded according to the reaction:

$$16\text{B} + 3\text{P}_2\text{O}_5 \rightarrow 6\text{BP} + 5\text{B}_2\text{O}_3.$$

Upon completion, the samples were cooled under nitrogen, washed with 10% NaOH solution to remove residual by-products, and subsequently dried. The obtained materials were comprehensively characterized by X-ray diffraction (XRD), scanning electron microscopy (SEM), and energy-dispersive X-ray spectroscopy (EDS). XRD analysis confirmed the formation of single-phase boron monophosphide (Figure 2), in full agreement with the PCPDF 110119 reference, exhibiting a zinc blende–type cubic structure with a lattice parameter of $a = 4.5380 \text{ \AA}$. SEM observations revealed uniformly distributed nanoparticles with an average particle size of about 80 nm (Figure 3). EDS analysis demonstrated a homogeneous distribution of boron and phosphorus with nearly equal atomic ratios throughout the sample (Figure 4). Overall, the results confirm that microwave irradiation enables the rapid, low-temperature synthesis of high-purity, single-phase boron

monophosphide nanopowder with a narrow particle-size distribution. **Lanthanide hexaborides:**

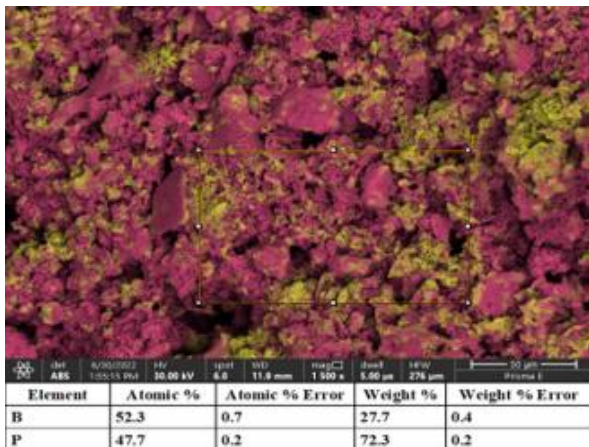
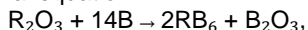


Figure 4. EDS mapping results of dried samples

Based on the characteristics of solid-state reactions under microwave irradiation and our previous experience in the synthesis of transition-metal borides and carbides, a series of lanthanide hexaborides ($R = \text{La, Ce, Pr, Nd, Sm, Gd, Ho, Er}$) were synthesized via microwave-assisted synthesis (MS). The reactions were performed using stoichiometric mixtures of lanthanide oxides and elemental boron according to the general equation:



with the exception of the CeO_2/B system. High-purity lanthanide oxides and boron powders were homogenized

and transferred into a quartz flow reactor, purged with high-purity helium, and irradiated in a modified domestic microwave oven (2.45 GHz, 900 W). Microwave heating was applied for 100–120 s until incandescence, followed by continued irradiation for 10 min. The temperature in the incandescence zone reached approximately 900–1050 °C, as measured by an optical pyrometer. After synthesis, the products were treated with dilute NaOH to remove residual B_2O_3 , thoroughly washed, filtered, and dried.

According to the results of the characterization of the synthesized RB_6 powders, it was shown that the series of lanthanides of our interest, from the point of view of microwave activated synthesis, can be divided into two subgroups: before gadolinium, at which hexaboride phases are obtained and after gadolinium when hexaborides are not formed, instead mixed boride phases were formed. Prior to microwave synthesis (MS) experiments, thermodynamic calculations were performed using the HSC Chemistry 10 software package. The calculated data are summarized in Table 1. As shown, for the most reactions between lanthanide oxides and boron, both the Gibbs free energy and Enthalpy changes exhibit positive values, indicating that these reactions are thermodynamically unfavorable under conventional conditions. This explains the need for extremely high temperatures in conventional synthesis routes. In contrast, the unique interaction between microwave irradiation and the reactants, enables the successful realization of these thermodynamically challenging reactions and the formation of lanthanide hexaborides (RB_6).

N	Reactions at 1100°C	ΔG kcal/mole	ΔH kcal/mole
1	$\text{La}_2\text{O}_3 + 14\text{B} = 2\text{LaB}_6 + \text{B}_2\text{O}_3$	+77.5	+70.8
2	$3\text{CeO}_2 + 22\text{B} = 3\text{CeB}_6 + 2\text{B}_2\text{O}_3$	-44.6	-37.1
3	$\text{Nd}_2\text{O}_3 + 14\text{B} = 2\text{NdB}_6 + \text{B}_2\text{O}_3$	+39.8	+55.8
4	$\text{Sm}_2\text{O}_3 + 14\text{B} = 2\text{SmB}_6 + \text{B}_2\text{O}_3$	+22.9	+38.8
5	$\text{Gd}_2\text{O}_3 + 14\text{B} = 2\text{GdB}_6 + \text{B}_2\text{O}_3$	+46.3	+77.0

Table 1. The value of the enthalpy and the change in the Gibbs free energy for the formation of hexaborides from the corresponding oxides and boron at 1100 °C.

Phase formation, crystallinity, and purity of the synthesized powders were primarily evaluated by X-ray diffraction (XRD). The diffraction patterns were analyzed using the Joint Committee on Powder Diffraction Standards (JCPDS) database and identified with MDI/JADE software. XRD results revealed that lanthanide hexaborides are predominantly formed for $R = \text{La, Ce, Pr, Nd, Sm}$,

and partially Gd. Specifically, intense diffraction peaks corresponding to cubic LaB_6 (PDF# 34-0427), CeB_6 (PDF# 38-1455), SmB_6 (PDF# 36-1326), PrB_6 (PDF# 38-1421), and NdB_6 (PDF# 65-1828) were observed. In some cases (LaB_6 , PrB_6 , NdB_6), weak reflections attributed to residual borate phases such as LaBO_3 (PDF# 12-0762), PrBO_3 (PDF# 23-1384), and $\text{Nd}(\text{BO}_2)_3$ (PDF# 23-1260) were detected (Figure 5).

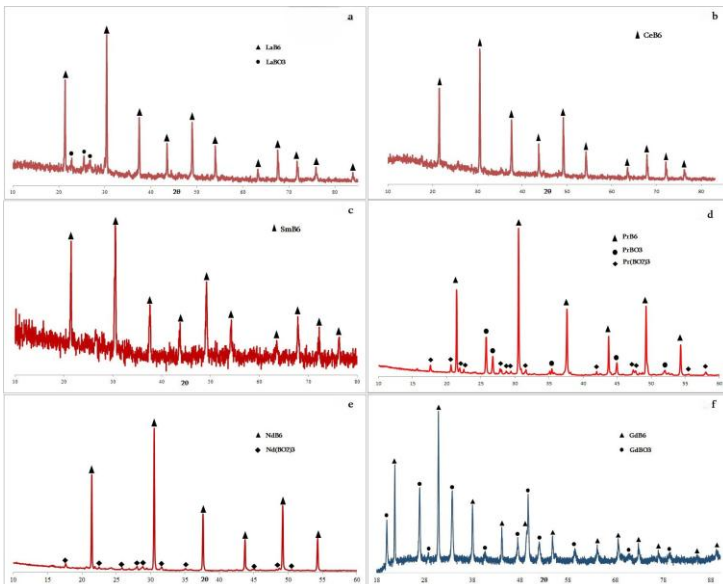


Figure 5. XRD patterns of the obtained RB_6 : a- LaB_6 ; b- CeB_6 ; c- SmB_6 ; d- PrB_6 ; e- NdB_6 ; f- GdB_6

confirming a clear limitation of hexaboride formation beyond Gd under identical microwave conditions. All synthesized hexaboride phases exhibited sharp and well-defined diffraction peaks (full width at half maximum $\approx 0.2^\circ$), indicative of high crystallinity and crystallite sizes exceeding 500 Å. The influence of microwave irradiation time on hexaboride formation was investigated using the $\text{La}_2\text{O}_3/\text{B}$ system under identical synthesis conditions. The reaction mixtures were irradiated for 0, 5, 10, 15, and 25 min, with the irradiation time counted from the onset of sample incandescence.

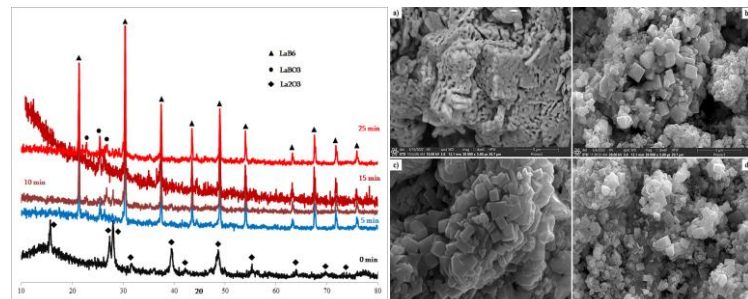


Figure 6. Comparative XRD patterns of LaB_6 samples irradiated at different time intervals (0; 5; 10; 15 and 25 minutes)-left; SEM images of LaB_6 samples irradiated at different time intervals: (a) – 0 min (initial mixture); b)-5 min.; c)-10 min. and d)-25 min.

For the $\text{Gd}_2\text{O}_3/\text{B}$ system, XRD analysis showed the coexistence of GdB_6 (PDF# 65-1823, 38-1424) with a significant fraction of GdBO_3 (PDF# 13-0483), indicating a reduction in hexaboride phase stability. For heavier lanthanides (Ho, Er), hexaborides were no longer the dominant phases; instead, mixed boride phases such as HoB_4 , HoB_{12} , ErB_4 , and ErB_{12} were formed,

Comparative XRD patterns (Figure 6) show that the LaB_6 phase forms within the first 5 min of irradiation, and neither peak intensities nor peak widths change significantly with further heating, indicating rapid phase formation and structural stabilization at early stages of microwave synthesis. SEM analysis confirmed

rapid crystal growth and well-defined cubic morphologies, with particle sizes typically in the 1–5 μm range (Figure 6).

Overall, the XRD and complementary analyses demonstrate that microwave-assisted synthesis enables rapid formation of highly crystalline lanthanide hexaborides, while also revealing intrinsic thermodynamic and kinetic limitations for heavier lanthanides.

Chapter 4. Microwave-assisted synthesis and investigation of catalytic properties of transition metal carbides (TMC): This chapter addresses the microwave-assisted synthesis of transition-metal-based nanocatalysts and their application in oxidative desulfurization and biomass-related hydrogenation reactions. The impact of synthesis parameters and design strategy on catalytic performance is systematically analyzed.

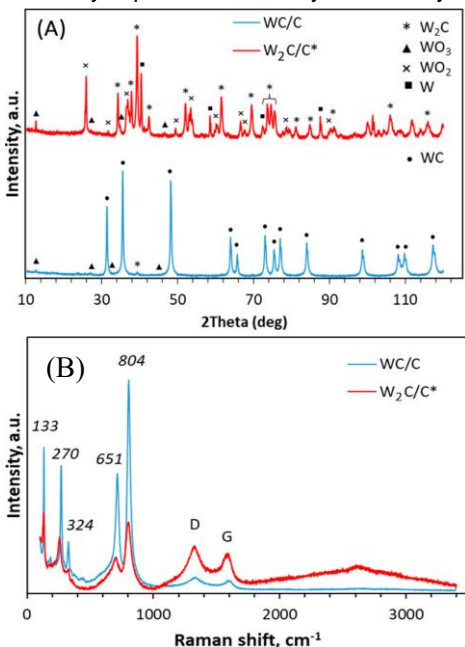


Figure 7. (A)-XRD patterns and (B)-Raman spectra of the samples

Microwave-Synthesized Tungsten Carbide as an Efficient Catalyst for Aerobic Oxidative Desulfurization: In recent years, tungsten carbide has attracted increasing attention as a functional catalytic material, particularly in oxidation-related processes such as methanol oxidation and hydrogen electro-oxidation. Despite its promising catalytic properties, the practical application of tungsten carbide remains limited by conventional synthesis routes, which typically require high temperatures, prolonged treatment times, and multistep procedures, resulting in elevated production costs.

In the present study, tungsten carbide supported on activated carbon was synthesized via a rapid microwave-assisted route, enabling catalyst preparation within 15 minutes. For the first time, it is demonstrated that microwave-synthesized tungsten carbide-based catalysts can be effectively employed in aerobic oxidative desulfurization, achieving efficient removal of diverse organosulfur compounds under mild reaction conditions.

Tungsten carbide supported on carbon (WC/C) was synthesized from WO₃ and Vulcan XC-72R carbon, which acted as both carbon source and microwave susceptor. The precursor mixture was prepared according to the reaction $\text{WO}_3 + 4\text{C} \rightarrow \text{WC} + 3\text{CO}$, with a slight excess of carbon (2.5 wt%), thoroughly

homogenized, and transferred to a quartz flow reactor. After degassing under flowing high-purity He (25 mL min⁻¹), the mixture was irradiated in a modified domestic microwave oven (2.45 GHz, 900 W) using a stepwise heating protocol followed by sustained irradiation to incandescence for 900 s. The synthesis temperature reached approximately 1150 °C, as measured by an infrared pyrometer. Helium flow was maintained during heating and cooling to prevent oxidation. The obtained WC/C catalyst was passivated at room temperature and subsequently activated in air at 120 °C and 6 atm for 2 h prior to catalytic testing. **Catalytic Tests:** Aerobic oxidative desulfurization was performed in a 40 mL steel autoclave using 0.5 wt% catalyst in a model sulfur-containing (DBT) solution (500 ppm S in decalin). Reactions were conducted under air with constant stirring (600 rpm) for 2 h at the desired temperature. After cooling, liquid products were analyzed by GC-FID using absolute calibration to determine sulfur conversion. The target catalyst

was obtained via rapid microwave synthesis of WC/C followed by controlled oxidative activation, yielding W_2C/C^* .

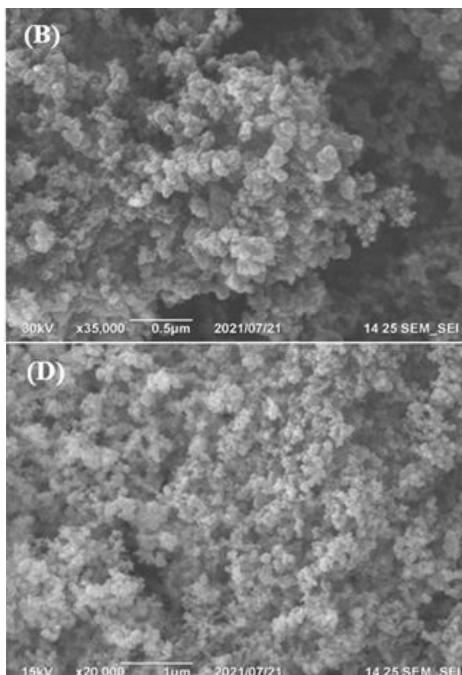
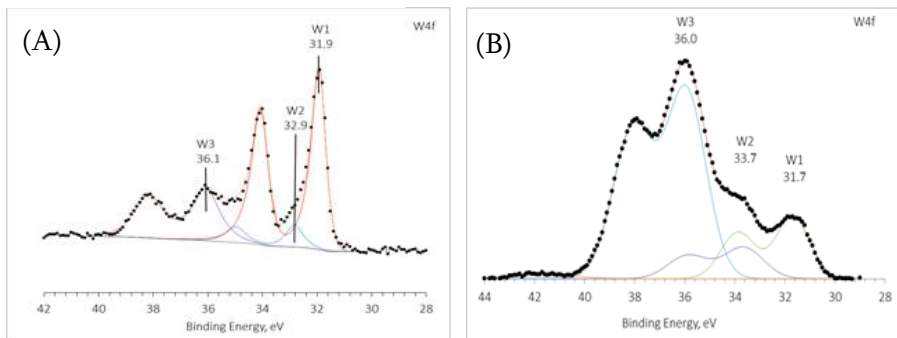


Figure 8. SEM micrographs of WC/C (B) and W_2C/C^* (D) samples

XRD analysis showed that the as-synthesized WC/C consists predominantly of hexagonal tungsten monocarbide, with characteristic reflections at $2\theta \approx 31.5^\circ, 35.6^\circ, 48.3^\circ, 64.0^\circ,$ and 73.0° , while only trace oxide-related signals were detected. After activation, the XRD pattern revealed the formation of a mixed surface-modified system containing tungsten sub-carbide (W_2C), metallic W, and tungsten oxides, with W_2C reflections appearing at $2\theta \approx 34.4^\circ, 37.9^\circ, 39.4^\circ,$ and 52.1° , and WO_2 -related reflections observed in the $2\theta \approx 26\text{--}38^\circ$ and $53\text{--}69^\circ$ ranges (Figure 7A). Raman spectra of the same samples exhibited bands at $\sim 133, 270, 324,$ and 804 cm^{-1} , assigned to W–C and W–O vibrational modes, alongside pronounced carbon D and G bands at ~ 1322 and 1584 cm^{-1} , respectively, indicating preserved graphitic carbon with moderate disorder (Figure 7B).

Nitrogen physisorption measurements showed type-II isotherms with H1 hysteresis loops for both samples. The BET surface area decreased only slightly from $\sim 14\text{ m}^2\text{ g}^{-1}$ for WC/C to $\sim 12\text{ m}^2\text{ g}^{-1}$ after activation, indicating that oxidation primarily affects surface chemistry rather than textural properties.

SEM analysis revealed a homogeneous granular morphology with particle sizes in the range of $\sim 50\text{--}90\text{ nm}$ (Figure 8).



Catalyst	Tungsten forms, quant., at. %		
	W1	W2	W3
WC/C	60.5	8	31.5

Figure 9. XPS spectra of W 4f regions of WC/C (A) and W_2C/C^* (B) samples and distribution of tungsten forms on the surface of the W_2C/C^* Catalysts

XPS analysis provided detailed insight into surface chemical states. Deconvolution of W 4f spectra revealed three tungsten species with W 4f_{7/2} binding energies at ~31.7–31.9 eV (carbide-like W⁰/WC_x), ~32.9–33.6 eV (partially oxidized W⁴⁺, assigned to WO₂ or tungsten oxycarbide), and ~36.1 eV (W⁶⁺, WO₃) (Figure 9). Oxidative activation reduced the fraction of carbide-type tungsten from ~60% to ~19%, while significantly increasing oxidized tungsten species.

The catalytic performance of microwave-synthesized tungsten carbide materials was evaluated in the aerobic oxidative desulfurization (ODS) of dibenzothiophene (DBT), a kinetically inert sulfur compound commonly used as a benchmark substrate. Comparative experiments demonstrated that pristine WC/C exhibits limited activity, while oxidative activation to form W₂C/C* markedly enhances DBT conversion, highlighting the critical role of tungsten in intermediate oxidation states for effective oxygen activation. Control experiments with carbon alone showed negligible activity, confirming that tungsten centers govern the oxidation process (Figure 10). Further catalyst optimized under varying reaction conditions. Catalyst stability under the applied experimental conditions was systematically evaluated through reusability (recycling) tests. The results demonstrate that the catalyst remains stable, retaining its catalytic efficiency over six consecutive cycles, with the conversion remaining essentially unchanged under batch conditions (Figure 11). Notably, the W₂C/C* catalyst achieved complete DBT oxidation within 3 h at 120 °C, outperforming most reported tungsten-based ODS systems, while requiring only 15 min for catalyst synthesis and 2 h for activation. This combination of rapid preparation, high efficiency, and operational stability underscores the advantages of microwave-assisted carbide synthesis for aerobic oxidative desulfurization. Microwave-assisted synthesis enables rapid (~15 min) preparation of tungsten carbide and its controlled activation to a W₂C/C* catalyst containing tungsten in an intermediate oxidation state (W⁴⁺), which effectively activates atmospheric oxygen. The catalyst exhibits high activity and stability in aerobic

Figure 10. Activity of catalysts in aerobic oxidation of DBT. conditions: 120 °C, catalyst dosage 0.5 wt %, 6 bar

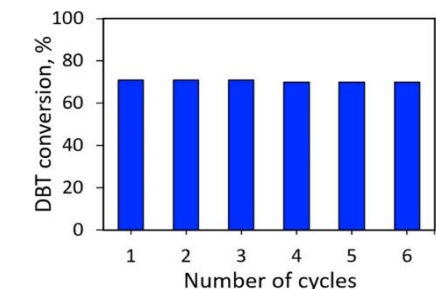


Figure 11. Oxidation of DBT with a regenerated catalyst. conditions: W₂C/C*-0.5 wt %, 120 °C, 6 bar, 2h

oxidative desulfurization, achieving 100% DBT conversion under mild conditions (120 °C, 6 bar air, 0.5 wt % catalyst, 3 h), with minimal changes in textural properties and stable performance over multiple reuse cycles.

Nanosized Mixed Fe–W Carbide Catalysts for Aerobic Oxidative Desulfurization of Fuels: In our previous work, microwave-synthesized tungsten carbide was shown to be an efficient catalyst for the aerobic oxidation of dibenzothiophene, with activity governed by surface tungsten species in intermediate oxidation states (W⁴⁺). However, partial oxygen consumption during carbide oxidation necessitated an additional activation step to achieve high catalytic performance. To overcome this limitation, iron was introduced as an oxygen-activating component via electron-transfer pathways. In this study, a nanosized mixed Fe–W carbide catalyst was synthesized for the first time by a single-step microwave method (15 min) and applied to aerobic oxidative

desulfurization. The FeWC catalyst exhibits high activity under mild conditions (120 °C, 2 h), does not require post-activation, and maintains stability over multiple reuse cycles. The role of iron in promoting radical-mediated oxygen activation and the influence of key reaction parameters are systematically investigated. A mixed Fe–W carbide catalyst was synthesized by microwave irradiation from a homogenized mixture of WO₃, FeO, and carbon. The precursor was treated in a quartz flow reactor under nitrogen and irradiated at 900 W, reaching ~1100 °C, with a total synthesis time of ~15 min, followed by cooling under inert atmosphere.

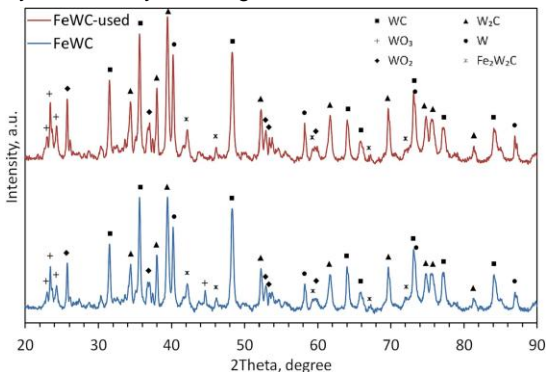


Figure 12. XRD pattern of fresh and used FeWC samples

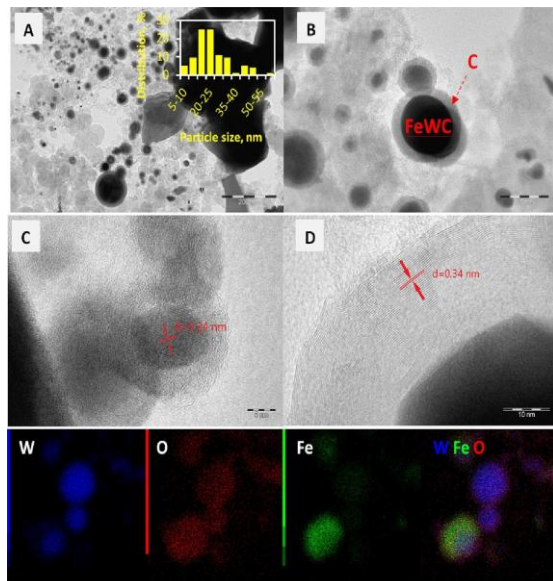


Figure 13. Microphotographs of fresh FeWC (A–C) sample and EDX mapping analysis

indicating excellent phase stability after at least five oxidative reaction cycles. Transmission electron microscopy reveals a nanosized “core–shell” morphology (Figure 13), where FeWC nanoparticles are uniformly dispersed within an amorphous carbon matrix. Particle size analysis shows a bimodal distribution with primary particles below 25 nm and agglomerates not exceeding 60 nm, with an average particle diameter of ~20 nm. High-resolution TEM images show lattice

irradiation from a homogenized mixture of WO₃, FeO, and carbon. The precursor was treated in a quartz flow reactor under nitrogen and irradiated at 900 W, reaching ~1100 °C, with a total synthesis time of ~15 min, followed by cooling under inert atmosphere.

Catalytic tests were carried out in a stirred steel autoclave using model sulfur compounds in decalin at 120 °C, air pressure of 2–8 bar, and catalyst loading of 0.5 wt%. Reaction products were analyzed by GC-FID. The catalyst performance was further evaluated in straight-run gasoline fractions at 130–170 °C using 2 wt% catalyst, with sulfur removal quantified by energy-dispersive X-ray analysis and detailed fuel composition assessed by GC×GC-TOFMS-FID.

X-ray diffraction analysis confirms that the microwave-synthesized FeWC catalyst is a multiphase system composed predominantly of tungsten carbides and metallic tungsten, accompanied by minor oxide and mixed carbide phases. The diffraction pattern exhibits intense reflections of hexagonal WC (JCPDS 89-2727) at $2\theta = 31.5^\circ$, 35.6° , and 48.3° , corresponding to the (001), (100), and (101) planes, respectively, together with orthorhombic W₂C (JCPDS 89-2371) characterized by reflections at 34.3° , 37.9° , 39.4° , 52.3° , and 61.6° . Metallic α -W (JCPDS 04-0806) is identified by peaks at 40.2° , 58.2° , 73.4° , and 86.9° . In addition, low-intensity reflections of monoclinic WO₂ (JCPDS 32-1393) and WO₃ (JCPDS 43-1035), as well as traces of mixed Fe₂W₂C (JCPDS 72-1987) and Fe₃O₄, are detected (Figure 12).

Importantly, XRD patterns of the fresh and used catalysts are nearly identical,

fringes with an interplanar spacing of 0.24nm, corresponding to WC (100) planes, while graphitic carbon layers with a spacing of ~ 0.34 nm ((002) graphite) surround the carbide cores. EDX mapping confirms a homogeneous spatial distribution of W and Fe, whereas oxygen is preferentially enriched at the particle surface, suggesting surface-localized oxide species.

Nitrogen adsorption–desorption measurements indicate a type II isotherm, characteristic of nonporous or weakly porous materials (Figure 14). The BET surface area of the fresh FeWC catalyst is $12.3 \text{ m}^2 \text{ g}^{-1}$, with a microporous contribution of $2.5 \text{ m}^2 \text{ g}^{-1}$ and an external surface area of $9.9 \text{ m}^2 \text{ g}^{-1}$. The average pore diameter does not exceed 9 nm, and no significant changes in textural properties are observed after repeated catalytic cycles, confirming structural robustness.

In addition, a fresh and used sample of the FeWC catalyst was analyzed by XPS to study the chemical composition and determine the relative oxidation states in the obtained samples (Figure 15). The W 4f spectra show three distinct tungsten states at binding energies of ~ 31.6 eV (WC_x /metallic W), 32.7 eV (W^{4+} , attributed to WO_2 or oxycarbide species), and 35.6 eV (W^{6+} , WO_3). High-resolution Fe2p curves indicate the coexistence of Fe^{2+} and Fe^{3+} species, with peaks at ~ 709.5 eV and ~ 710.8 eV, respectively. Quantitative XPS analysis demonstrates that graphite carbon dominates the surface composition ($\sim 79\%$), with a slight decrease after reuse, while the fraction of oxygen-containing species and hydroxyl groups increases. Notably, the $\text{Fe}^{3+}/\text{Fe}^{2+}$ ratio approximately doubles after catalytic operation, indicating the active participation of iron species in redox cycling and electron transfer during oxygen activation. Simultaneously, the gradual decrease of WC_x surface species suggests partial surface oxidation

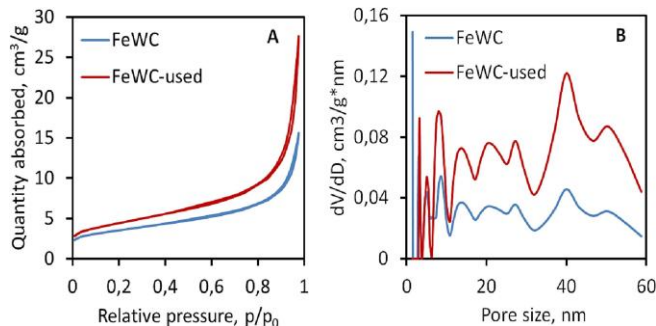


Figure 14. Nitrogen adsorption–desorption isotherms (A) and pore size distribution curves (B).

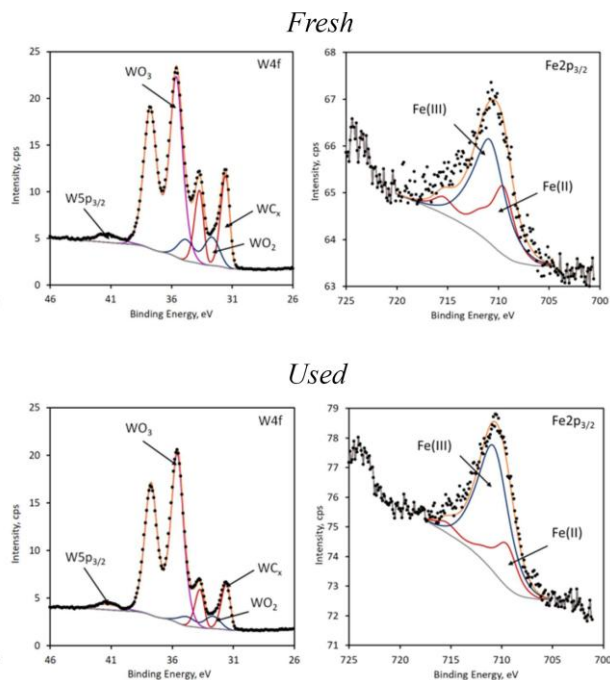


Figure 15. W4f and Fe2p profiles spectra of fresh and used FeWC samples: high-resolution curves of (A) C1s, (B) O1s, (C) W4f and (D) Fe2p.

under reaction conditions, consistent with XRD observations. Overall, the combined XRD, electron microscopy, adsorption, and spectroscopic results demonstrate that the FeWC catalyst consists of stable nanosized carbide cores embedded in a conductive carbon matrix, with surface-localized mixed-valence tungsten and iron species. This unique structural and electronic configuration enables efficient oxygen activation without the need for a separate activation step, distinguishing FeWC from conventional WC-based catalysts and underpinning its high catalytic performance in aerobic oxidative desulfurization.

The catalytic performance of the mixed tungsten–iron carbide (FeWC) was evaluated in the

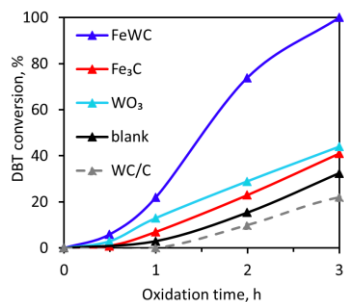


Figure 16. Catalytic performance of various carbide materials. Reaction condition: total sulfur 500 ppm, 0.5 wt%, 120°C, 6 atm.

aerobic oxidative desulfurization of dibenzothiophene (DBT, 500 ppm S) using air as the oxidant. The catalyst design is based on a synergistic concept combining iron sites responsible for oxygen activation and radical initiation with oxidized tungsten species capable of forming active peroxy/dioxo complexes for sulfur oxidation. Unlike monometallic tungsten carbide, where oxygen is partially consumed for surface oxidation and requires a separate activation step, incorporation of iron enables in situ oxygen activation via electron transfer, eliminating the need for preliminary catalyst activation. Under optimized conditions (120 °C, 6 atm air), the FeWC catalyst achieved complete DBT removal within 3 h, demonstrating markedly higher activity than monometallic systems, for which DBT conversion did not exceed 22% for WC/C and 40% for Fe₃C under identical conditions (Figure 16). These results clearly confirm the synergistic interaction between Fe and W

centers in the mixed carbide catalyst.

Reaction parameters were systematically optimized. The FeWC catalyst exhibited excellent stability over five consecutive cycles, with unchanged DBT conversion (Figure 17A). FTIR analysis confirmed structural integrity (Figure 17B), while UV–Vis spectroscopy with 8-hydroxyquinoline showed no Fe leaching (Figure 17C,D), demonstrating the robustness of the mixed carbide catalyst under oxidative conditions.

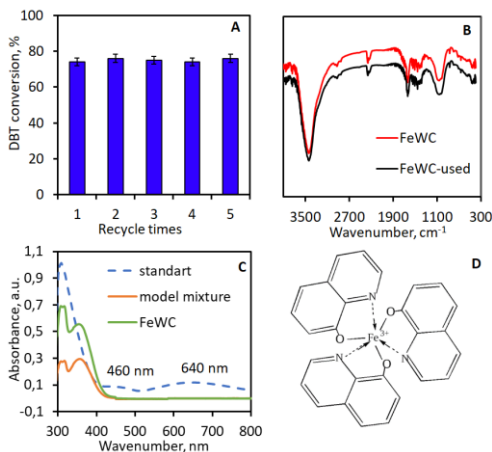


Figure 17. Recycle catalyst (A). Reaction conditions: total sulfur 500 ppm, 0.5 wt.% catalyst, 120°C, 6 atm, 2 h, (B) FT-IR spectra of FeWC before and after five runs, (C) Absorption spectrum of standard solution, model mixture before and after oxidative reaction in the presence of FeWC, (D) 8-hydroxyquinoline-Iron complex.

The applicability of the FeWC catalyst was further validated in the aerobic oxidative desulfurization of real straight-run petroleum fractions. A straight-run gasoline fraction (160–200 °C, 995 ppm S) was treated via a two-stage oxidation–extraction protocol using air as the oxidant. Under the optimal temperature of 150 °C enabled a reduction of sulfur content to 6 ppm after the second oxidation stage, corresponding to >99% sulfur removal.

Fuel quality analysis demonstrated that key parameters such as density and water content remained unchanged, while the octane number increased slightly (from 53 to 55), consistent with the formation of trace oxygenated species. The FeWC catalyst also exhibited high efficiency in straight-run diesel desulfurization, reducing sulfur content from 3800 ppm to 64 ppm (>98%) after two oxidation cycles under comparable conditions. Overall, these results confirm the high efficiency, selectivity, and industrial relevance of the FeWC catalyst for aerobic oxidative desulfurization of real petroleum fuels under mild conditions.

Microwave-Assisted Synthesis of Nanosized Molybdenum Carbide and Its Catalytic Performance in Naphthalene Hydrogenation:

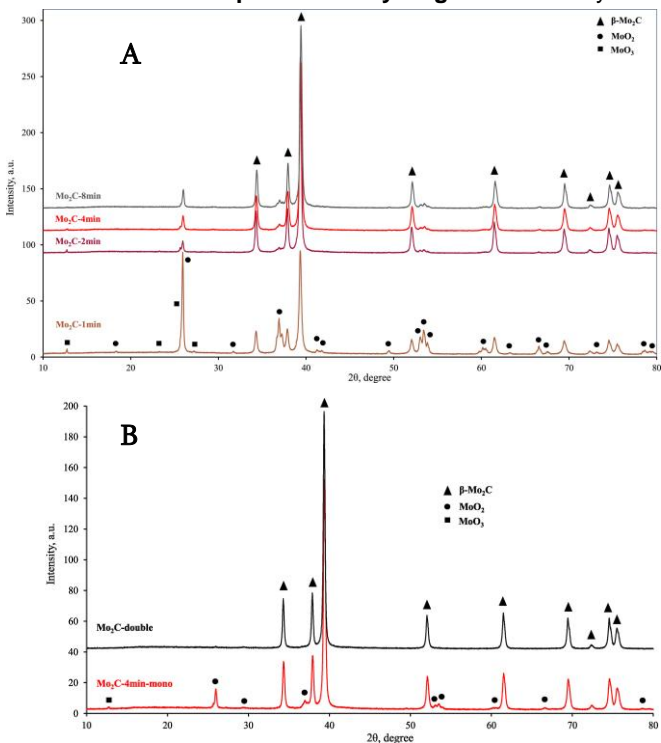


Figure 18. A-The XRD patterns of series samples obtained at different MW irradiation times; B-XRD patterns of pure phase β -Mo₂C after secondary MW irradiation

naphthalene was performed in a 50 mL stainless-steel autoclave using 50–300 mg of catalyst and a 1 wt% naphthalene solution in dodecane. After hydrogen charging, reactions were conducted under stirring (350 rpm) at controlled temperature and pressure. Reaction products were analyzed by GC-FID. Catalyst stability was evaluated through multiple reuse cycles with intermediate washing and re-testing under identical conditions.

transition-metal carbide catalyst for high-temperature processes and has attracted increasing interest for low-temperature catalytic applications. Notably, molybdenum carbides exhibit noble-metal-like activity in hydrogen-involved reactions while offering superior resistance to catalyst poisoning.

Molybdenum carbide (Mo₂C) was synthesized by microwave-assisted method using MoO₃ and Vulcan XC-72R carbon according to the stoichiometric reaction MoO₃ + 7C → Mo₂C + 6CO. Row mixture was homogenized by magnetic stirring and mortar grinding, and transferred to a quartz flow reactor. The reactor was purged with nitrogen (99.99%) and irradiated (1–8 min time intervals) in a microwave oven at 900 W until incandescence. The reaction temperature (≈1050–1150 °C) was monitored by an optical pyrometer, and nitrogen flow (25 mL min⁻¹) was maintained throughout synthesis. Catalytic hydrogenation of

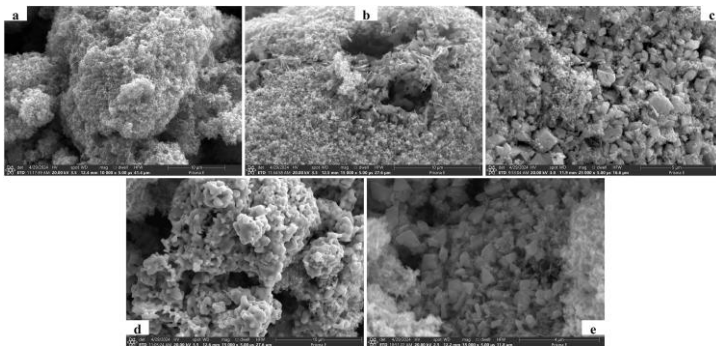
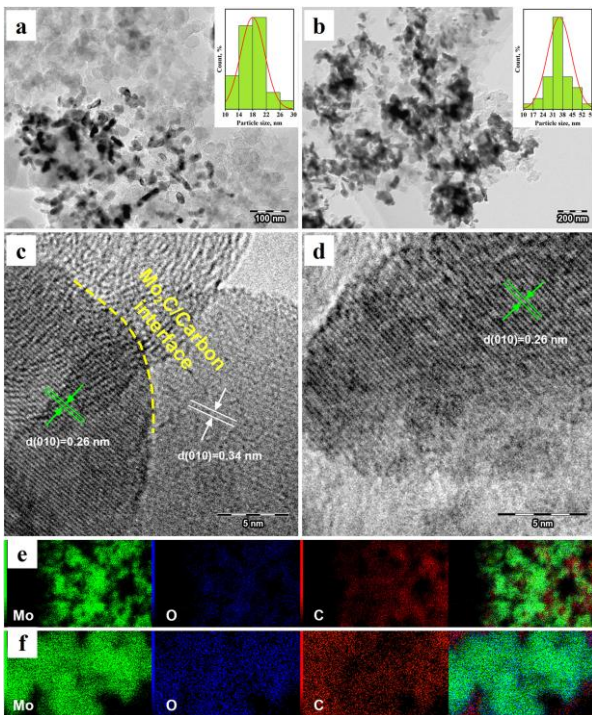


Figure 19. The SEM images of a series of samples obtained at different MW irradiation times: a - 1 min (Mo_2C -1 min); b - 2 min (Mo_2C -2 min); c - 4 min (Mo_2C -4 min-mono); d - 8 min (Mo_2C -8 min) and e-secondary irradiated for additional 4 min (Mo_2C -double).



Under microwave irradiation, the selective formation of $\beta\text{-Mo}_2\text{C}$ was achieved. To elucidate phase evolution and its impact on catalytic behavior, a temporal microwave synthesis study was performed using a stoichiometric $\text{MoO}_3\text{-C}$ mixture irradiated for 1, 2, 4, and 8 min (Figure 18A). XRD analysis shows that $\beta\text{-Mo}_2\text{C}$ (PDF# 35-0787) already forms after 1 min, constituting ~40–50% of the sample, alongside MoO_2 (PDF# 65-5787) and trace MoO_3 (PDF#35-0609).

Figure 20. TEM images for Mo_2C -4 min-mono (a) and Mo_2C -double (b) samples (the insets show particle size distribution); (c, d)-HR-TEM images of Mo_2C -4 min-mono and Mo_2C -double samples accordingly and (e, f) the corresponding mapping analysis of Mo, C and O elements for Mo_2C -4 min-mono and Mo_2C -double samples accordingly.

Increasing irradiation time enhances carbide formation while oxide reflections diminish. After 4 min, a predominantly $\beta\text{-Mo}_2\text{C}$ phase is obtained with residual MoO_2 , which persists even after 8 min, indicating a sequential reduction pathway $\text{MoO}_3 \rightarrow \text{MoO}_2 \rightarrow \text{Mo}_2\text{C}$. The 4 min sample is denoted Mo_2C -4min-mono. Prolonged irradiation alone does not eliminate MoO_2 due to inhomogeneity induced by rapid gas evolution during the initial irradiation stage, leading to partial carbon migration from the reaction zone. To overcome this limitation, the Mo_2C -4min-mono sample was re-homogenized and re-irradiated for an additional 4 min, yielding a phase-pure $\beta\text{-Mo}_2\text{C}$ material (Mo_2C -double). XRD patterns (Figure 18B) show only characteristic $\beta\text{-Mo}_2\text{C}$

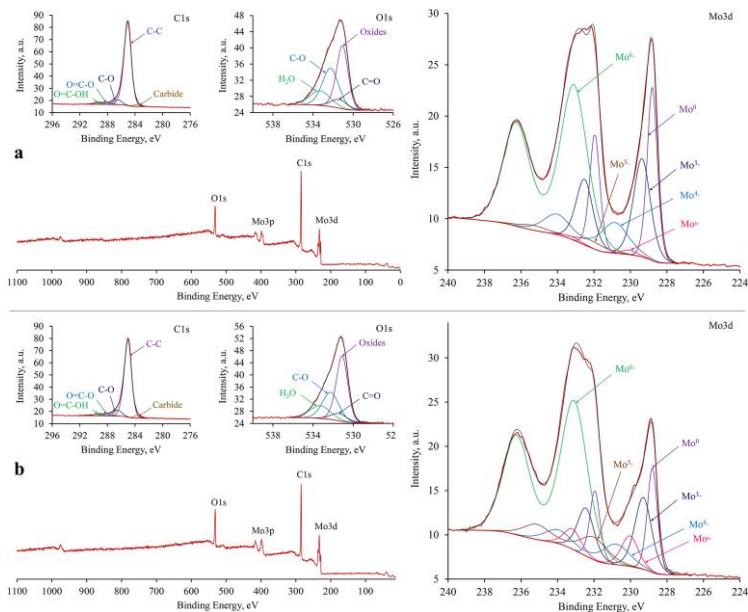


Figure 21. The wide and Mo3d, C1s, O1s XPS spectra for Mo₂C-4 min-mono (a) and Mo₂C-double (b) samples.

reflections at 34.32°, 37.9°, 39.35°, 52.09°, 61.52°, 69.5°, 74.6°, and 75.6°, corresponding to the (100), (002), (101), (102), (110), (103), and (112) planes of the hcp structure. Both mono- and double-treated samples exhibit high crystallinity (FWHM ≈ 0.22°). Crystallite sizes estimated by the Scherrer equation are ~15.6 nm (Mo₂C-4min-mono) and ~33 nm (Mo₂C-double), consistent with TEM results. SEM-EDS analysis (Figure 19a-e) reveals uniform particle distribution and porous microstructures formed as early as 1 min irradiation, with micropores of 12–15

nm, later confirmed by N₂-adsorption/desorption analysis. Particle morphology remains largely unchanged up to 4 min, while 8 min irradiation induces agglomeration. Taking all the above into account further detailed investigation was conducted with the samples of Mo₂C-4 min-mono and Mo₂C-double.

TEM images (Figure 20 a, b) show homogeneously distributed nanoparticles with spherical and rod-like morphologies. Average particle sizes are 17 ± 2 nm (Mo₂C-4min-mono) and 35 ± 2 nm (Mo₂C-double), confirming XRD trends. HRTEM of Mo₂C-double (Fig. 20c) shows lattice fringes with d = 0.26 nm corresponding to β-Mo₂C (010) planes. In contrast, Mo₂C-4min-mono also exhibits fringes at 0.34 nm assigned to graphitic carbon (002), indicating incomplete carburization, consistent with residual oxides observed by XRD. EDX mapping (Figure 20 e, f) confirms homogeneous Mo and C distribution, while oxygen is enriched at particle surfaces, more prominently in Mo₂C-double, in agreement with XPS results. Surface oxygen originates both from residual oxides and rapid air oxidation forming surface oxycarbides.

To show the electronic structure and surface oxidation states of Mo, C, and O in the Mo₂C-4min-mono and Mo₂C-double catalysts, XPS analysis was performed. The Mo 3d core-level spectra (Figure 21 a, b) display well-resolved Mo 3d_{5/2} and 3d_{3/2} doublets, revealing multiple molybdenum oxidation states, including Mo⁰, Mo³⁺, Mo⁴⁺, Mo⁵⁺, Mo⁶⁺, and Mo^{δ+} (2 < δ < 4). The dominant species follow the trend Mo⁶⁺ > Mo⁰ > Mo³⁺ > Mo⁴⁺ > Mo^{δ+} > Mo⁵⁺. Doublets at 228.6/232.1 eV and 229.3/232.4 eV are assigned to Mo⁰ and Mo³⁺, corresponding to Mo–Mo and Mo–C bonds in β-Mo₂C. Peaks at 230.7/234.0 eV indicate Mo⁴⁺ (MoO₂), while higher binding-energy components at 232.0/235.1 eV and 233.0/236.0 eV correspond to Mo⁵⁺ and Mo⁶⁺, arising from surface oxidation and residual oxide species; more pronounced in Mo₂C-4min-mono, consistent with XRD data.

The intermediate $\text{Mo}^{\delta+}$ state at 229.9/233.1 eV is attributed to surface oxycarbide species. Notably, $\text{Mo}^{\delta+}$ and Mo^{5+} contributions are significantly higher in Mo_2C -double, latter suggests that secondary irradiation of the sample increases the number of active sites for oxygen adsorption.

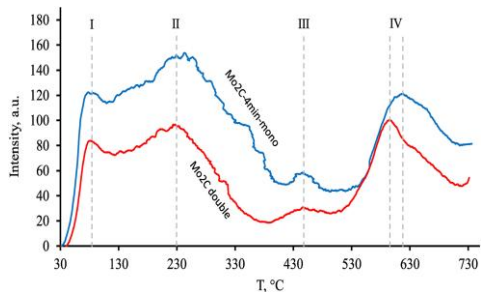


Figure 22. NH_3 -TPD profiles of Mo_2C -4 min-mono and Mo_2C -double

Furthermore, TEM analysis of the Mo_2C -4min-mono samples has shown that the Mo_2C nanoparticles are encapsulated by a carbon shell (Figure 20 a and c). This carbon coating is assumed to mitigate further oxidation when the nanoparticles are exposed to air oxygen. Despite these differences, BET surface areas of Mo_2C -4min-mono ($10.7 \text{ m}^2 \text{ g}^{-1}$) and Mo_2C -double ($10.5 \text{ m}^2 \text{ g}^{-1}$) are nearly identical, confirming that XPS intensity variations originate from chemical effects rather than surface-area differences. C 1s spectra (Figure 21 a, b) include a carbide-related peak at 283.3 eV and higher-binding-energy components at 285.1–289.3 eV attributed to C–C, C–O, O=C–O, and O=C–OH species, confirming partial surface oxidation. The O 1s spectra further support the presence of lattice oxides and adsorbed oxygen species.

NH_3 -TPD profiles (Figure 22) reveal four desorption peaks at ~ 80 , ~ 230 , ~ 450 , and ~ 600 °C. The first three peaks are attributed to Brønsted acid sites, while the high-temperature peak corresponds to Lewis acid sites. Mo_2C -4min-mono exhibits stronger overall acidity, whereas Mo_2C -double shows a higher proportion of surface Lewis sites, consistent with its increased concentration of intermediate Mo oxidation states observed by XPS.

Catalytic hydrogenation of naphthalene over β - Mo_2C catalysts: Blank experiments conducted at 350 °C and 4.0 MPa H_2 for 2 h confirmed that naphthalene hydrogenation does not proceed in the absence of a catalyst (Figure 23), indicating a negligible non-catalytic contribution.

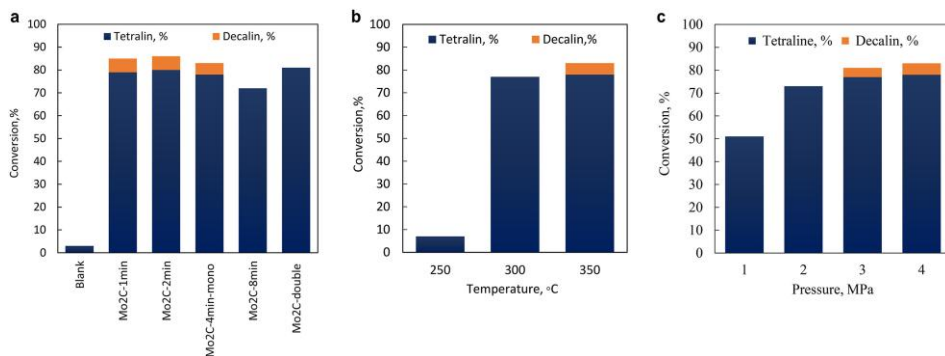


Figure 23. Synthesis time impact on catalyst performance (a); Effect of reaction temperature (b) and hydrogen pressure on naphthalene conversion (c) over Mo_2C -4 min-mono catalyst. Reaction conditions for (a) and (b): naphthalene concentration 1 %, catalyst amount 100 mg (3.3 wt%), 350°C, hydrogen pressure 4.0 MPa, 1h., stirring 350 rpm, for (c): naphthalene concentration 1 %, catalyst amount 100 mg (3.3 wt%), 350°C, 1h., stirring 350 rpm.

The catalytic performance of β - Mo_2C samples synthesized under different microwave irradiation times was evaluated using naphthalene hydrogenation as a model reaction (350 °C, 4.0 MPa H_2 ,

1 h, 100 mg catalyst). In all cases, comparable overall naphthalene conversion was achieved; however, significant differences in product selectivity were observed (Figure 23a). Catalysts synthesized for shorter durations (1–4 min) exhibited markedly higher selectivity toward decalin, indicating deeper hydrogenation, whereas samples prepared for longer times showed suppressed decalin formation. This behavior correlates with the phase and surface composition of the catalysts. Shorter synthesis times preserve molybdenum oxide species with higher Mo oxidation states, as confirmed by XPS and NH₃-TPD (Figures 21 and 22), which provide acidic sites facilitating aromatic ring coordination. In contrast, prolonged synthesis (8 min) leads to oxide depletion and particle agglomeration (SEM, Figure 19e), resulting in reduced conversion and negligible deep hydrogenation. Thus, the coexistence of carbide (H₂ activation) and oxide-derived acidic sites enables dual functionality, consistent with previous reports on acidity-enhanced naphthalene hydrogenation.

Although XRD shows phase-pure β -Mo₂C for Mo₂C-double samples (Figure 18B), XPS reveals a higher fraction of intermediate Mo^{δ+}/Mo⁵⁺ species (Figure 21b). Despite similar overall conversion, these catalysts did not produce decalin, confirming that deep hydrogenation requires specific oxide phases with higher Mo oxidation states integrated into the surface structure.

Reaction parameters further were systematically optimized using Mo₂C-4 min-mono catalyst. Lowering the temperature to 300 °C slightly reduced conversion, while at 250 °C hydrogenation was negligible (Figure 23b), consistent with literature thresholds for Mo₂C catalysts. Hydrogen pressure strongly affected activity: optimal performance was achieved at 30–40 atm, whereas

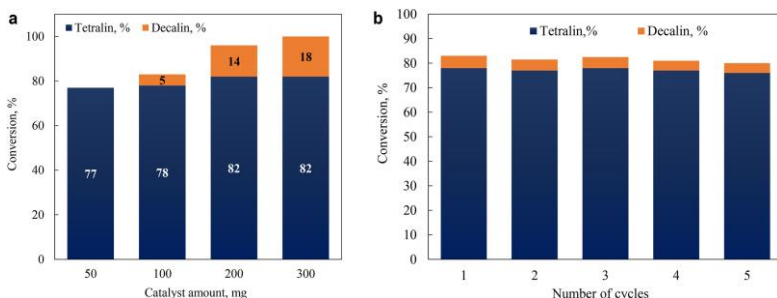


Figure 24. Influence of Mo₂C-4 min-mono catalyst dosage on naphthalene conversion (a) and recycle/reuse of Mo₂C-4 min-mono catalyst (b); Reaction conditions: naphthalene concentration 1 %, hydrogen pressure 4.0 MPa, 350 °C, 1h., stirring 350 rpm.

conversion dropped to ~55 % at 10 atm due to reduced hydrogen solubility in dodecane (Figure 23c).

Catalyst loading also influenced both conversion and selectivity (Figure 24a). Increasing the amount from 50 to 300 mg raised conversion from ~80 % to 100 % and promoted decalin formation.

At lower loadings (50 mg), naphthalene was selectively hydrogenated to tetralin, demonstrating that product distribution can be tuned via catalyst dosage. Notably, such high tetralin selectivity is typically associated with noble-metal catalysts (Pt, Pd), highlighting β -Mo₂C as a cost-effective alternative.

Recycling experiments confirmed excellent catalyst stability. Mo₂C-4 min-mono retained both conversion and decalin selectivity over at least five consecutive cycles without regeneration (Figure 24b), demonstrating robust structural and catalytic stability.

In this study, catalyst efficiency is primarily evaluated based on the total conversion of naphthalene under fixed reaction conditions. This approach enables a straightforward comparison of catalyst performance by examining both naphthalene conversion and product selectivity under standard conditions. The reactions were conducted under conditions commonly reported in the literature for

naphthalene hydrogenation, facilitating direct comparison of the obtained conversion and selectivity values with previously reported data.

Conclusions

1. For the first time, microwave-assisted solid-state synthesis was successfully applied to the preparation of lanthanide-series hexaborides and boron monophosphide.
2. Microwave-synthesized transition-metal carbides were developed, and the decisive influence of synthesis parameters on their phase composition, surface states, and catalytic activity was clearly demonstrated.
3. Mixed carbide nanocatalysts (Fe–W–C) were synthesized for the first time, exhibiting a pronounced synergistic effect in aerobic oxidative desulfurization reactions.
4. The FeWC catalyst demonstrated high efficiency in the aerobic oxidative desulfurization of real petroleum fractions under mild conditions, maintaining excellent stability over at least six reuse cycles.
5. Hydrogenation studies over molybdenum carbide revealed that catalyst selectivity (tetralin vs decalin formation) can be effectively tuned by controlling microwave synthesis conditions.
6. Microwave-assisted synthesis was shown to be an efficient alternative to conventional high-temperature furnace-based methods, enabling ultrashort synthesis times, controlled nanostructures, and broad prospects for practical catalytic applications.

Published papers:

1. Aghoyan, A.; Akopyan, A. V.; Aleksanyan, G.; Davtyan, D. Microwave-Assisted Synthesis and Catalytic Activity of Nano-Sized Molybdenum Carbide in Naphthalene Hydrogenation. *Heliyon* 2025, 11 (3), e42431. <https://doi.org/10.1016/j.heliyon.2025.e42431>
2. Aghoyan, A. M. Microwave-Assisted Synthesis of Lanthanide Hexaborides: Formation of LaB₆, PrB₆ and Challenges with Heavier Lanthanides. *Proc. Yerevan State Univ., Chem. Biol.* 2025, 59 (3), 84–94. <https://doi.org/10.46991/PYSUB.2025.59.3.084>
3. Mnatsakanyan, R.; Aghoyan, A.; Adamyan, R.; Kharatyan, S.; Akopyan, A. V.; Davtyan, D. Rapid Microwave-Assisted Synthesis of Rare-Earth Hexaboride Powders. *Adv. Appl. Ceram.* 2024, 123 (4–6), 97–101. <https://doi.org/10.1177/17436753241302225>
4. Akopyan, A. V.; Eseva, E. A.; Mnatsakanyan, R. A.; Davtyan, D. A.; Lukashov, M. O.; Levin, I. S.; Sadovnikov, A. A.; Anisimov, A. V.; Terzyan, A. M.; Agoyan, A. M.; Karakhanov, E. A. Catalytic Aerobic Desulfurization of Fuels in the Presence of Nanosized Mixed Carbide FeWC. *Chem. Eng. J.* 2023, 464, 142641. <https://doi.org/10.1016/j.cej.2023.142641>
5. Mnatsakanyan, R.; Aghoyan, A.; Davtyan, D. Microwave-Assisted Synthesis of Boron Monophosphide Nanopowder. *Ceram. Int.* 2023, 49 (2), 3066–3069. <https://doi.org/10.1016/j.ceramint.2022.10.330>
6. Akopyan, A. V.; Mnatsakanyan, R. A.; Eseva, E. A.; Davtyan, D. A.; Polikarpova, P. D.; Lukashov, M. O.; Levin, I. S.; Cherednichenko, K. A.; Anisimov, A. V.; Terzyan, A. M.; Agoyan, A. M.; Karakhanov, E. A. New Type of Catalyst for Efficient Aerobic Oxidative Desulfurization Based on Tungsten Carbide Synthesized by the Microwave Method. *ACS Omega* 2022, 7 (14), 11788–11798. <https://doi.org/10.1021/acsomega.1c06969>

Արթուր Մանվելի Աղոյան

ՈՐՈՇ ԱՆՑՈՒՄԱՅԻՆ ՇԱՐՔԻ ՄԵՏԱՂՆԵՐԻ (IV-VI) ՆԱՆՈՉԱՓԱԿԱՆ ԿԱՐՔԻՂՆԵՐԻ ԵՎ ԼԱՆՁԱՆԱՅԻՆ ՇԱՐՔԻ ՄԵՏԱՂՆԵՐԻ ԲՈՐԻՂՆԵՐԻ ՄԻԿՐՈԱԼԻԷԱՅԻՆ ՄԻՆԹԵՉ ԵՎ ԿԱՏԱԼԻՏԻԿ ՉԱՏՎՈՒԹՅՈՒՆՆԵՐԻ ՈՒՍՈՒՄՆԱՍԻՐՈՒԹՅՈՒՆ Ամփոփագիր

Աշխատանքի նպատակն է եղել միկրոալիքային ճառագայթման կիրառմամբ սինթեզել լանթանային շարքի մետաղների հեքսաբորիդներ և բորի մոնոֆոսֆիդ, ինչպես նաև անցումային մետաղների (IV-VI) խառը և դոպացված կարբիդներ: Կիրառված սինթեզի մեթոդը թույլ է տվել ստանալ վերջիններիս նանոֆազերը, մասնիկների չափսերի նեղ բախշվածության տիրույթով: Ստացված նյութերը փորձարկվել են երկու ուղղությամբ՝ որպես հետերոգեն կատալիզատորներ և որպես կարծր նյութեր:

Սինթեզի համար կիրառվել է կենցաղային միկրոալիքային վառարանը, որը հնարավորություն է տվել ապահովելու ռեակցիոն խառնուրդի առավելագույն ճառագայթում՝ իներտ հոսքային միջավայրում: Ռեակցիոն խառնուրդի ջերմաստիճանը միկրոալիքային ճառագայթման պայմաններում չափվել է հեռահար ինֆրակարմիր (Dostman HT 1800) ջերմաչափով:

Ստացված նյութերի կառուցվածքը և տեքստուրային առանձնահատկություններն ուսումնասիրվել են բազմաթիվ ֆիզիկոքիմիական եղանակներով (XRD, SEM/EDS, TEM/EDX, XPS, H₂-TPR, NH₃-TPD, BET և այլն):

Աշխատանքի արդյունքում սինթեզվել են հետևյալ նյութերի նանոֆազերը լանթանային մետաղների հեքսաբորիդներ/բորիդներ՝ RB₆ (R=La, Ce, Sm, Nd, Pr, Gd, Ho, Er), BP, WC/C, FeWC, Mo₂C:

Ստացված նյութերը որպես կատալիզատորներ փորձարկվել են հետևյալ ռեակցիաներում՝ արենների հիդրում, դեհիդրում, դիզելային վառելիքում պարունակվող ծծումբօրգանական միացությունների աերոբիկ օքսիդացմամբ ծծմբազրկում և այլն:

Ստացվել են հետևյալ արդյունքները.

1. Առաջին անգամ միկրոալիքային սինթեզի եղանակով իրականացվել է լանթանային մի շարք մետաղների հեքսաբորիդների և բորի մոնոֆոսֆիդի սինթեզ:
2. Մշակվել են միկրոալիքային սինթեզով ստացված անցումային մետաղների կարբիդներ, որոնց համար ապացուցվել է սինթեզի պայմանների վճռորոշ ազդեցությունը դրանց ֆազային բաղադրության և մակերեսային ակտիվության վրա:
3. Առաջին անգամ ստացվել են խառը կարբիդային նանոկատալիզատորներ (Fe-W-C)՝ դրսևորելով հստակ սիներգետիկ էֆեկտ աերոբ օքսիդատիվ ծծմբազրկման ռեակցիաներում:
4. Ցույց է տրվել, որ FeWC կատալիզատորը արդյունավետ է մեղմ պայմաններում իրական նավթային ֆրակցիաների աերոբ օքսիդատիվ ծծմբազրկման համար՝ ցուցաբերելով բարձր կայունություն կատալիզատորի վերօգտագործման վեց ցիկլերում:
5. Մոլիբդենի կարբիդի կիրառմամբ իրականացված հիդրման ուսումնասիրությունները ցույց են տվել, որ հնարավոր է կարգավորել կատալիզատորի ընտրողականությունը (տետրալին/դեկալին) սինթեզի պայմանների փոփոխման միջոցով:
6. Ցույց է տրվել, որ միկրոալիքային սինթեզը հանդիսանում է ավանդական բարձր ջերմաստիճանային դասական մեթոդներին արդյունավետ այլընտրանք, ապահովելով սինթեզի գերկարճ ժամանակներ, վերահսկելի նանոկառուցվածք՝ ապահովելով կիրառական մեծ հեռանկար:

**МИКРОВОЛНОВЫЙ СИНТЕЗ И КАТАЛИТИЧЕСКИЕ СВОЙСТВА НАНОРАЗМЕРНЫХ
КАРБИДОВ НЕКОТОРЫХ ПЕРЕХОДНЫХ МЕТАЛЛОВ (IV–VI) И БОРИДОВ МЕТАЛЛОВ
ЛАНТАНОВОГО РЯДА**

Резюме

Целью работы был синтез гексаборидов металлов лантанового ряда и монофосфида бора, а также смешанных и допированных карбидов переходных металлов (IV–VI) с использованием микроволнового излучения. Примененный метод синтеза позволил получить нанофазы последних с узким распределением частиц по размерам. Полученные материалы были исследованы в двух направлениях: в качестве гетерогенных катализаторов и в качестве твердых материалов.

Для синтеза использовалась специально модифицирована бытовая микроволновая печь, что позволило обеспечить максимальное облучение реакционной смеси в инертной проточной среде. Температура реакционной смеси в условиях микроволнового облучения измерялась с помощью дистанционного инфракрасного термометра (Dostman HT 1800). Структура и текстурные особенности полученных материалов изучались многочисленными физико-химическими методами (XRD, SEM/EDS, TEM/EDX, XPS, H₂-TPR, NH₃-TPD, BET и др.).

В результате работы были синтезированы нанофазы следующих материалов: гексабориды/бориды металлов лантана: RB₆ (R=La, Ce, Sm, Nd, Pr, Gd, Ho, Er), BP, WC/C, FeWC, Mo₂C.

Полученные материалы были протестированы в качестве катализаторов в следующих реакциях: гидрирование, дегидрирование аренов, десульфуризация путем аэробного окисления органических соединений серы, содержащихся в дизельном топливе, и др.

Были получены следующие результаты:

1. Впервые синтез ряда гексаборидов лантана и монофосфида бора был осуществлен с использованием микроволнового синтеза.
2. Были разработаны карбиды переходных металлов, полученные микроволновым синтезом, для которых было доказано решающее влияние условий синтеза на их фазовый состав и поверхностную активность.
3. Впервые были получены смешанные карбидные нанокатализаторы (Fe–W–C), демонстрирующие явный синергетический эффект в реакциях аэробной окислительной десульфуризации.
4. Было показано, что катализатор FeWC эффективен для аэробной окислительной десульфуризации реальных нефтяных фракций в мягких условиях, демонстрируя высокую стабильность в шести циклах повторного использования катализатора.
5. Исследования гидрировании с использованием карбида молибдена показали, что селективность катализатора (тетралин/декалин) можно регулировать изменением условий синтеза.
6. Было показано, что микроволновый синтез является эффективной альтернативой традиционным высокотемпературным классическим методам, обеспечивая сверхкороткое время синтеза и контролируемые наноструктуры, что открывает большие перспективы применения.